Z. Phys. B - Condensed Matter 86, 359-365 (1992)

Condensed Matter
Zeitschrift für Physik B

The boundary condition integration technique: results for the Hubbard model in 1D and 2D

Claudius Gros*

Institut für Physik, Universität Dortmund, Postfach 500 500, W-4600 Dortmund 50, Federal Republic of Germany

Received July 15, 1991; revised version September 23, 1991

We study models of strongly correlated electrons in one- and two dimensions. We exactly diagonalize small clusters with general boundary conditions (BC) and integrate over all possible BC. This technique recovers the kinetic energy part of the (extended lattice) Hamiltonian *exactly* in a grand-canonical formulation. A continuous range of particle densities may be described with this technique and the momentum space can be probed for arbitrary momenta. For the Hubbard Hamiltonian we recover details of the Mott-insulating behaviour for the momentum distribution function at half filling, both in 1D and 2D. Off half-filling the shape of the *canonical* Fermi surface is strongly distorted in 2D with respect to the *grand canonical* Fermi surface. The shape of the grand canonical Fermi surface obtained by this finite-size technique reduces in the weak-coupling limit exactly to that of the infinite-lattice Fermi sea.

Introduction

Effective one-band models, like the Hubbard and the $t-J$ model, have been studied intensively in recent times. These studies are partly motivated by the discovery of the high-temperature superconductors and, as a consequence of them, our understanding of the 1D Hubbard and $t-J$ models has progressed considerably. In particular, the *Tomonaga-Luttinger liquid* [1], realized in 1D [2], has drawn the attention of many physicists. The momentum-distribution function in the ground state, $n(k) \equiv \langle c_k^\dagger c_k \rangle_0$, of a Tomonaga-Luttinger liquid has the characteristic form

$$n(k) = \tfrac{1}{2} + C|k-k_F|^\alpha \operatorname{sgn}(k-k_F), \qquad (1)$$

for momentum k near the Fermi-momentum, k_F, α being a non-universal critical exponent and C a constant. The 1D infinite-U Hubbard model has rigorously been shown to behave as a Tomonaga-Luttinger liquid [3, 4, 5]. In 2D the situation is less clear. Anderson's hypothesis [6] that an analogous behaviour to the 1D case is to be expected in two spatial dimensions, has not yet been substantiated. A diagrammatic expansion in exponentially low densities [7] has resulted in a standard Fermi-liquid behaviour. In this paper we will investigate the prospect of exact diagonalization procedures to shed light on this issue.

It is not easy to extract information on properties in momentum space from diagonalization studies of small, real-space clusters. Generally, for a cluster with N_s sites, only N_s k-states can be probed in momentum space and properties near the Fermi-surface (like (1)) are difficult to access. The Bethe-Ansatz equations for the 1D Hubbard model in the infinite-U limit have been solved for chains up to 32-sites [8] and a direct confirmation that (1) holds has been possible. For the 1D $t-J$ model no analytic solution is known apart from $J/t = 0, 2$ [9] and the ground state is accessible by numerical methods only for chains with up to 16 sites. This length is not enough to probe (1) directly, but the use of a geology relation [3], between the compressibility and the critical exponent, α, made possible a study of the Tomonaga-Luttinger behaviour [10]. Consistent results have been obtained by a recent variational formulation [11].

It has been pointed out previously that other than periodic boundary conditions (BC) might in certain cases improve the accuracy the results obtained from exact diagonalization of small clusters. In particular the variation in energy with system size can be minimized by an appropiate choice [12, 13] of the BC or by integration [14, 15] over all possible BC. Here we explore this technique in more detail and apply it to the Hubbard model for finite and infinite U in 1D and 2D. We will present results for the momentum distribution function, $n(k)$, and discuss the limitations of this technique.

Technique

Translational invariant many-body hamiltonians consist of two parts. The kinetic energy term, diagonal in mo-

* email: UPH 301 at DDOHR Z11

mentum space, and the interaction term, diagonal in real space. The choice of the basis used to formulate a given approach will generally determine which of the two terms is treated more throughly. The standard Green's function approach in momentum space takes the kinetic energy term exactly into account, insofar as the non-interacing limit is recovered rigorously. It is now possible to reformulate the exact diagonalization of small clusters in terms of a conserving approximation in the language of perturbation theory. To be concrete, let us consider the one-band Hubbard Hamiltonian in one or two spatial dimensions,

$$H = -t \sum_{\sigma, \langle i,j \rangle} (c^{\dagger}_{i,\sigma} c_{j,\sigma} + c^{\dagger}_{j,\sigma} c_{i,\sigma}) + U \sum_{i} n_{i,\uparrow} n_{i,\downarrow} . \tag{2}$$

Here $c^{\dagger}_{i,\sigma}, c_{i,\sigma}$ and $n_{i,\sigma} = c^{\dagger}_{i,\sigma} c_{i,\sigma}$ are the creation/anihilation and the particle number operators on site i of fermions with spin $\sigma = \uparrow, \downarrow$, respectively. $t > 0$ is the hopping matrix element between nearest neighbor sites, $\langle i, j \rangle$; $U \geqq 0$ is the onsite Coulomb repulsion. We consider (2) on a finite cluster with general boundary conditions. For illustration we consider a square cluster with periodicity N_x and N_y (The lattice constant is set to unity throughout this paper.) in x- and y-directions respectively and impose the general boundary condition

$$\begin{aligned} \psi(x + N_x, y) &= e^{i\alpha_x} \psi(x, y) \\ \psi(x, y + N_y) &= e^{i\alpha_y} \psi(x, y) \end{aligned} \tag{3}$$

on the one-particle wavefunction $\psi(x, y)$. (The many-body wavefunction has to obey (3) for every argument). $\alpha_{x,y} = 0, \pi$ correspond to periodic and antiperiodic boundary conditions, respectively. The eigenstates of (2) in the non-interacting limit, $U = 0$, are given by plane waves of the form $\psi(x, y) = \exp[i(k_x x + k_y y)]/\sqrt{N_x N_y}$. The positions of the $\mathbf{k}$-vectors are determined via the boundary conditions:

$$\begin{aligned} k_x &= \frac{\alpha_x + 2\pi m_x}{N_x}, \quad m_x = 0, \ldots, N_x - 1 \\ k_y &= \frac{\alpha_y + 2\pi m_y}{N_y}, \quad m_y = 0, \ldots, N_y - 1 . \end{aligned} \tag{4}$$

We allowed values of k_x, k_y form a rigid grid of $N_s = N_x \times N_y$ points which is shifted by the boundary conditions, α_x, α_y. By varying $\alpha_x \in [0, 2\pi[$ the *complete* Brillouin zone is sampled by the grid of the N_s allowed $\mathbf{k} \equiv (k_x, k_y)$ values. In Fig. 1 we show for illustration the case for a 4×4 system. The 16 (open and filled) circles are the positions of the $\mathbf{k}$'s in the Brillouin zone, for a given set of boundary conditions α_x, α_y. By varying $\alpha_x, \alpha_y \in [0, 2\pi[$ the filled circles will cover the shaded region, which covers 1/16 of the Brillouin zone. Also shown in Fig. 1 is the Fermi-surface at half-filling (dashed-point line), which encloses 8 $\mathbf{k}$'s. The N_s discrete Energy-levels are given by

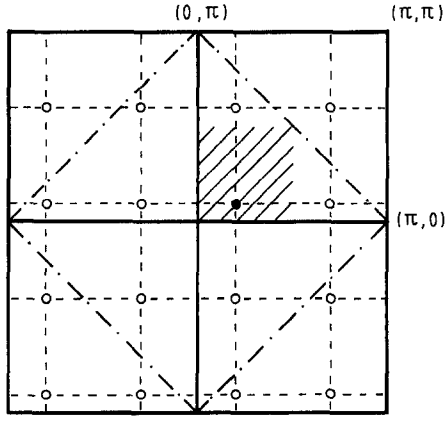

Fig. 1. The position of the $\mathbf{k}$'s (open and filled circles) in the first Brillouin zone for a 4×4 cluster with general boundary conditions. When we vary the boundary conditions between $[0, \pi[$ the $\mathbf{k}$ denoted by the filled circles will cover the hatched region, 1/16 of the Brillouin zone

$$\varepsilon(\mathbf{k}) \equiv -2t \left[\cos\left(\frac{\alpha_x + 2\pi m_x}{N_x} \right) + \cos\left(\frac{\alpha_y + 2\pi m_y}{N_y} \right) \right], \tag{5}$$

where on the right side of the equality $\mathbf{k}$ has been substituted by its value given by (4). For a numerical diagonalization study it is convenient to perform a gauge transformation to the Fermi-operators $c_{(x,y),\sigma} \rightarrow \exp[-i(x\alpha_x/N_x + y\alpha_y/N_y)] c_{(x,y),\sigma}$. Consequently the diagonalization of the $N_x \times N_y$ cluster considered is done with *periodic* boundary conditions *and* a phase-dependent hopping matrix element $-t_{(x,y),(x',y')} = -t \exp[i(x - x')\alpha_x/N_x + i(y - y')\alpha_y/N_y]$.

The results of the non-interacting ($U = 0$) *and* thermodynamic limit, are recovered *exactly* in a grand-canonical formulation of the boundary condition integration technique on a finite lattice *and* and average over $\alpha_x, \alpha_y \in [0, 2\pi[$. The (grand canonical) ground state energy and the particle density per site are given by

$$\begin{aligned} e(\mu) &= \frac{1}{N_s} \int_0^{2\pi} \frac{d\alpha_x d\alpha_y}{(2\pi)^2} \sum_{m_x, m_y = 0}^{N_x, N_y} (\varepsilon(\mathbf{k}) - \mu)\, \theta(\mu - \varepsilon(\mathbf{k})) \\ n &= \frac{1}{N_s} \int_0^{2\pi} \frac{d\alpha_x d\alpha_y}{(2\pi)^2} \sum_{m_x, m_y = 0}^{N_x, N_y} \theta(\mu - \varepsilon(\mathbf{k})), \end{aligned} \tag{6}$$

where $\mathbf{k}$ is given by (4). μ is the chemical potential and $\theta(\varepsilon)$ is the step function. ($\theta(\varepsilon) = 0$, 1/2, 1 for $\varepsilon < 0, = 0, > 0$ respectively.) The canonical ground-state energy, given by the Legendre transform [14] $e(n) = \sup_{\mu} (e(\mu) + \mu n)$, is just the energy of the (here 2D) Fermi-sea.

The real-space interaction, $U > 0$, on the finite $N_x \times N_y$ cluster corresponds in momentum space to scattering from any $\mathbf{k}$ to any other $\mathbf{k}'$ of the allowed $N_x \times N_y$ discrete momenta given by (4) (see also Fig. 1), for the same α_x, α_y. In the language of diagrams, the scattering between

this discrete set of allowed **k**'s summed up to all orders, vertex corrections included.

Let's denote with $E_{(\alpha_x,\alpha_y),N_e}$ the total (canonical) ground-state energy for the cluster considered with N_e particles. The (grand-canonical) ground-state energy and particle density per site is then given for the general, interacting case by

$$e(\mu)=\frac{1}{N_s}\int_0^{2\pi}\frac{d\alpha_x d\alpha_y}{(2\pi)^2}\times\inf_{N_e}(E_{(\alpha_x,\alpha_y),N_e}-\mu N_e) \tag{7}$$

In practise, the integrals over the boundary conditions in (7) are approximated by a finite sum. We typically choose between $N_b=20,\ldots 120$ different boundary conditions and diagonalize the cluster as many times. A total of $N_s\times N_b$ different **k**'s are then included in the calculations. We will use the notation $N_s:N_s\times N_b$ for such a cluster, where the first index stands for the number of sites in real-space and the second index for the number of sites in momentum-space. For example a 8:480 cluster is one with 8-sites (in real-space) diagonalized for 60 different boundary condition (which we choose to be evenly distributed between $[0,2\pi[$). A 8:8 cluster is just the exact solution for the 8-site problem with one definite boundary condition only.

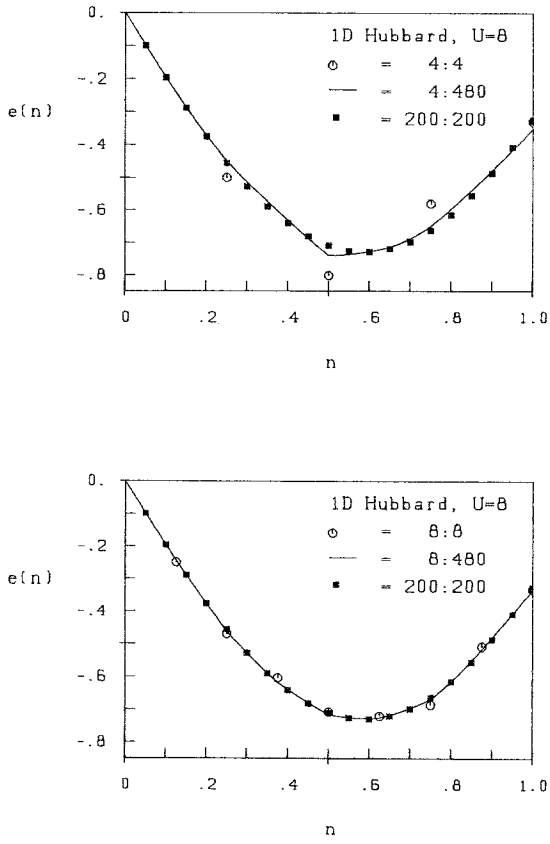

Fig. 2a, b. The ground-state energy per site, $e(n)$ (in units of t), for 1D Hubbard chains and $U=8$. The continuous line is the result for chains with (**a**) 4 sites in real space, 480 in momentum space (4:480) and (**b**) 8 sites in real space, 480 in momentum space (8:480). The data for chains with only periodic boundary conditions: (**a**) the 4:4 cluster, (**b**) the 8:8 cluster, are denoted by the open symbols. Also shown is the Bethe-Ansatz result, obtained from chains of length 200 (the 200:200 cluster)

Results

We will first discuss results for the ground-state energy in 1D where we can compare with Bethe Ansatz results and then present results for the momentum distribution function in 1D and 2D. In 1D the boundary condition integration technique yields the exact ground-state energy in both the $U=0$ and the $U=\infty$ limit. For a test of the method we therefore consider an intermediate $U=8$. We have diagonalized with a modified Lanczos method chains with $N_s=4$, 8 sites and particle number N_e ranging from 1 to N_s. For the 4-site chain we have averaged over 120 boundary conditions (a 4:480 cluster) and for the 8-site chain over 60 boundary conditions (a 8:480 cluster). The ground-state energy per site, $e(n)$ (in units of t), as a function of density, n, is plotted in Fig. 2 (continuous line). For comparison, we have indicated with the open symbols the data for the corresponding cluster with only periodic boundary conditions (the 4:4 and 8:8 system). Also shown in Fig. 2 is an estimate of the ground-state energy of the infinite chain as obtained by the diagonalization of a 200-site chain, with periodic BC, via the Bethe-Ansatz equation. Clearly, the integration over boundary conditions reduces in magnitude the finite size corrections to the ground-state energy.

In addition, a (nearly) continuous set of densities can be described with the boundary condition technique, whereas a fixed boundary condition diagonalization recovers only densities being multiples of $1/N_s$, corresponding to $N_e=1, 2,\ldots$. Some finite size corrections to the boundary condition integration data are still discernible and manifest themselves most prominently in some kinks in the otherwise continuous curves, e.g. at $n=0.5$ for the 4:480 chain. For most densities, the average over particle numbers, N_e, is important insofar as more than one value of N_e contributes to (7). But at certain densities $1/N_s$ (0, 0.25, 0.5,... for the 4-site chain and 0, 0.125, 0.25,... for the 8-site chain) the canonical and the grand-canonical average are identical and only one value of N_e has to be considered. This property is closely related to the fact, that in 1D the Fermi-surface is uniquely determined by the particle densities. In 2D the particle density determines only the volume enclosed by the Fermi surface and the shape of the Fermi surface is (as we will discuss below) strongly size dependent in a canonical study (with fixed particle number). In 2D the average over particle number has always to be done off half-filling, only at half filling does in 2D the canonical and the grand-canonical representation coincide.

The momentum distribution function, $n(\mathbf{k})$, is defined via $n(\mathbf{k})=1/2\langle c^\dagger_{\mathbf{m},\uparrow}c_{\mathbf{m},\uparrow}+c^\dagger_{\mathbf{m},\downarrow}c_{\mathbf{m},\downarrow}\rangle_0$ where the relation between the momentum, **k**, and $\mathbf{m}\equiv(m_x,m_y)$ is given by

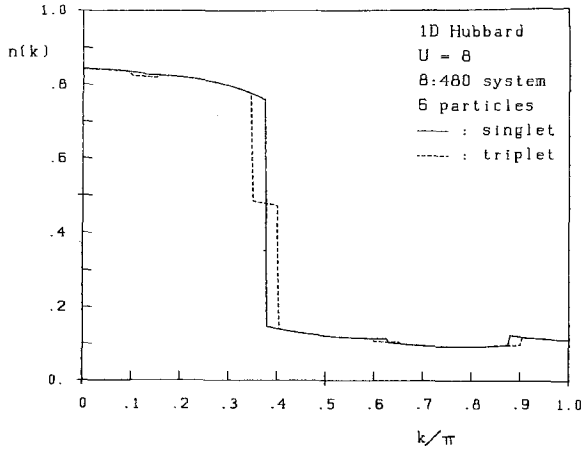

Fig. 3. The momentum distribution function, $n(k)$, as a function of momentum (in units of π) for a 1D Hubbard chain ($U=8$) with 8 sites and 6 particles. The momentum distribution in the grond-state of the spin singlet subspace is given by the continuous line. The overall ground-state (with no total-spin constraint) becomes a triplet near the Fermi-surface (dashed line)

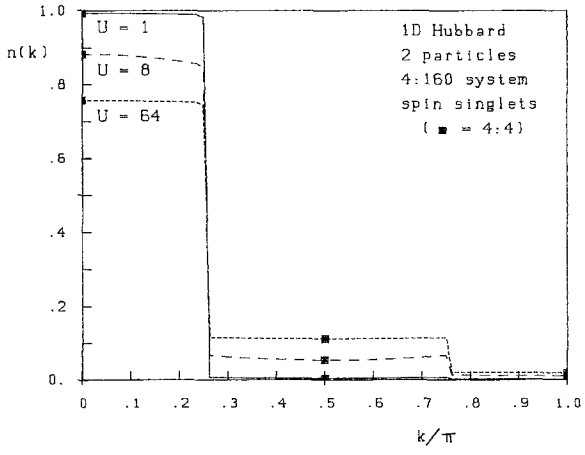

Fig. 4. The momentum distribution function, $n(k)$, as a function of k (in units of π) for a one dimensional 4:160 system (4 site chain, 40 different boundary conditions) at quarter filling ($N_e=2$ particles) and $U=1$, 8, 64 (smooth curves). Note the discontinuity at the Fermi-edge (at $k_F=\pi/4$); the Tomonaga-Luttinger behaviour expected in the thermodynamic limit is not recovered [17]. Also shown (square symbols) are the data points for the 4:4 chain (four sites, periodic boundary conditions only)

(4) and $\langle\ \rangle_0$ denotes the expectation value in the N_e-particle ground-state of the cluster. We consider only clusters with identical number of up- and down spins. First we discuss a generic result.

In Fig. 3 we present $n(k)$ as obtained from the diagonalization of a 8:480 Hubbard chain with $U=8$ and six particles. In this system, a level crossing occurs between a spin-singlet and a triplet (dashed line). The solid line in Fig. 3 is the data for $n(k)$ when the diagonalization is performed within the subspace of total spin singlets. (In the Appendix we explain the projection technique used to handle the contraint of fixed total spin.) The transition to a triplet state near the Fermi-surface, which occurs when the total spin is not kept fixed, is due to non-filled shells near the Fermi-surface and is closely related to oscillations of ground-state properties as a function of chain-length which have been considered previously in 1D in the context of the periodic Anderson [12] and Hubbard [13, 8] models and in 2D in the context of the Gutzwiller wavefunction [16] (see also [14]).

The phenomenon of ferromagnetism at the Fermi-edge is even more pronounced in 2D. Four **k** vectors are degenerate in the case of periodic BC. When these states are only partially filled, multiple level-crossings into high spin states occur as a function of boundary conditions and therefore also as a function of momentum, **k** (compare (4)). Here we are not interested in the question of ferromagnetism and all the data presented below for $n(k)$ will be for ground-states in the subspace of spin-singlets.

In Fig. 4 we present $n(k)$ for a 4:160 chain (4 sites, 40 different boundary conditions) with 2 particles (corresponding to quarter filling) and $U=1$, 8, 64, as a function of k (in units of π). As a consequence of the interaction the values of $n(k)$ is suppressed for $k<k_F$ and enhanced for $k>k_F$. $n(k)$ drops somewhat from $k=0$ towards the Fermi-edge but a finite discontinuity is observed [17] (This behaviour is generic for densities $n<1$.) at the Fermi-edge, and the Tomonaga-Luttinger behaviour (see Eq. (1)) expected for the ground-state in the thermodynamic limit is not recovered. Also shown in Fig. 4 are the data for the respective 4-site chain with periodic boundary conditions only (square symbols).

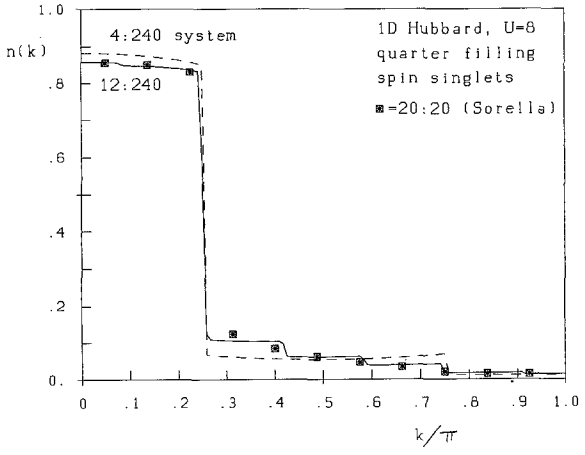

Fig. 5. The momentum distribution function, $n(k)$, as a function of k (in units of π) at quarter filling and $U=8$ and a 4:240 chain with $N_e=2$ particles and a 12:240 chain with $N_e=6$ particles. Note the spurious discontinuities in $n(k)$ due to the discreteness of the clusters. These discontinuities decrease in size with increasing chain length. Also included is data for a 20-site chain [18] (square symbols)

In Fig. 5 we present $n(k)$ at quarter filling and $U=8$ for a 4:240 chain with 2 particles (dashed line) and a 12:240 chain with 6 particles (continuous line). With increasing chain-length spurious discontinuities of decreasing magnitude occur in $n(k)$ at momenta $n'\pi/N_s + \pi/(2N_s)$ ($n'=1,\ldots N_s/2$). We also included in Fig. 5 the data for $n(k)$ obtained from a 20-site chain [18] (square symbols) with 10 particles.

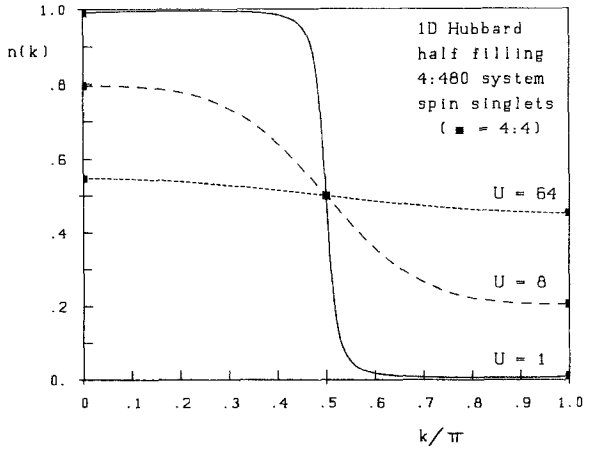

Fig. 6. The momentum distribution function, $n(k)$, as a function of k (in units of π) for a 4:480 chain (4 site chain, 120 boundary conditions) at half filling ($N_e=4$ particles) and $U=1$, 8, 64 (smooth curves). Note the absence of a discontinuity at the Fermi-edge, indicative of an insulating state. Also shown (square symbols) are the data points for the 4:4 chain (four sites, periodic boundary conditions only)

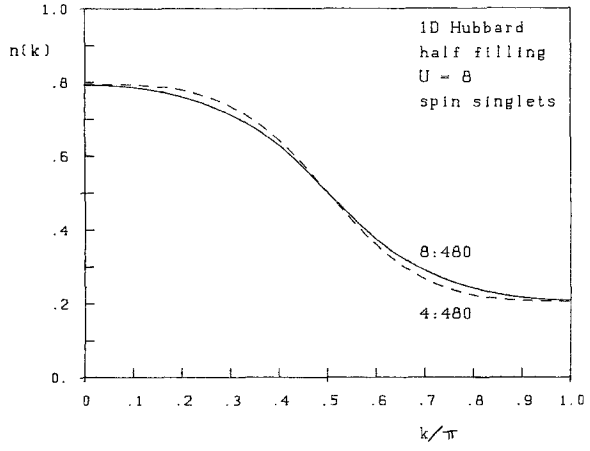

Fig. 7. Comparison between the momentum distribution function, $n(k)$, as a function of k (in units of π) for 4:480 (dashed curve) and 8:480 (continuous curve) Hubbard chains (4 and 8 sites, 120 and 60 boundary conditions respectively) at half filling with $U=8$. The difference between the two curves yields an estimate of the (quantitative) finite-size corrections to $n(k)$, which are smaller than 5%. This estimate is supported also by a comparison with Monte-Carlo data [19].

In Fig. 6 we present $n(k)$ for a 4:480 cluster with 4 particles and $U=1$, 8, 64. At half-filling an insulating state is expected, as it is born out by the data. $n(k_F=\pi/2)=0.5$ exactly (due to particle-hole symmetry), no discontinuity occurs at the Fermi-edge and the slope of $n(k)$ through the Fermi-edge is linear. Also shown in Fig. 6 are the data for the respective 4-site chain with periodic boundary conditions only (4:4 system, square symbols).

In Fig. 7 we compare $n(k)$ for a 4:480 chain and an 8:480 chain (4 and 8 real-space sites, 480 sites in momentum space) at half-filling and $U=8$. The difference between the two curves yields an estimate of the finite-size corrections of $n(k)$ as calculated by the boundary

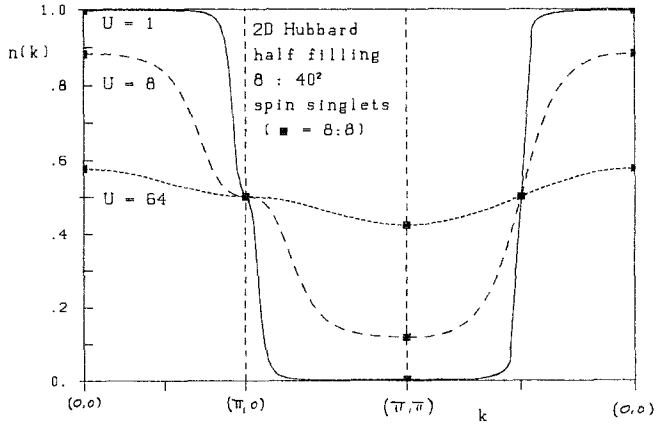

Fig. 8. The momentum distribution function, $n(\mathbf{k})$, for a 2D, half-filled Hubbard cluster, with 8 sites and $1600=40^2$ different boundary conditions. The smooth curves are the data for $n(\mathbf{k})$ along $(0,0)\rightarrow(\pi,0)\rightarrow(\pi,\pi)\rightarrow(0,0)$ in the Brillouin zone for $U=1$, 8, 64. Note the absence of a discontinuity at the Fermi-edge (at $(0,\pi)$ and $(\pi/2,\pi/2)$), indicative of an insulating state and the *linear* versus *quadratic* behaviour of $n(k)-1/2$ near the Fermi-edge along the (1, 1) and the (1, 0) direction respectively. Also shown (square symbols) are the data points for the corresponding 8:8 cluster (eight sites, periodic boundary conditions only)

condition technique. Qualitatively the curves do not change with chain length, quantitatively the difference is less than 5%. We compared the data presented in Fig. 5 with those obtained from Monte-Carlo simulations [19] and found agreement within ~5%. This degree of agreement supports the our estimate of the finite-size corrections.

In Fig. 8 we present $n(k)$ for an $8:40^2$ two-dimensional Hubbard cluster at half-filling ($N_e=8$ particles) and various U. The cluster is such that it tiles the square lattice by periodicity through translations of (2, 2) and (−2, 2). The momentum distribution is shown for a cut through the Brillouin zone along $(0,0)\rightarrow(0,\pi)\rightarrow(\pi,\pi)\rightarrow(0,0)$ (compare with Fig. 1). Again, as in 1D at half-filling, no discontinuity occurs at the Fermi edge, here at $(0,\pi)$ and $(\pi/2,\pi/2)$, indicative of an insulating behaviour of the ground-state. Note the anisotropy of $n(k)$ at the Fermi surface, where $n(\mathbf{k}_F)=1/2$ exactly. Along the (1, 1) direction $n(k,k)-1/2$ passes *linearly* through the Fermi edge and *quadratically* along the (1, 0) direction, due to the saddle point in the kinetic energy. Also shown in Fig. 8 are the data points for the respective 8-site cluster with periodic boundary conditions only (square symbols). Although the cluster corresponds nominally to an $8:40^2$ (8:1600) system, only $60=3\times20=3\times(40/2)$ different boundary conditions have actually been evaluated in order to obtain the data presented in Fig. 8. This is possible since clusters with different BC are diagonalized independently. In general, one will diagonalize only clusters with boundary conditions appropiate to the **k**-values (compare Eq. (4)) one is interested in.

In Fig. 9 we present data for the same 2D cluster with 8 sites in real space and 80^2 BC, $U=8$ and ∞ and a fixed number of particles $N_e=2$ (a canonical study). This cor-

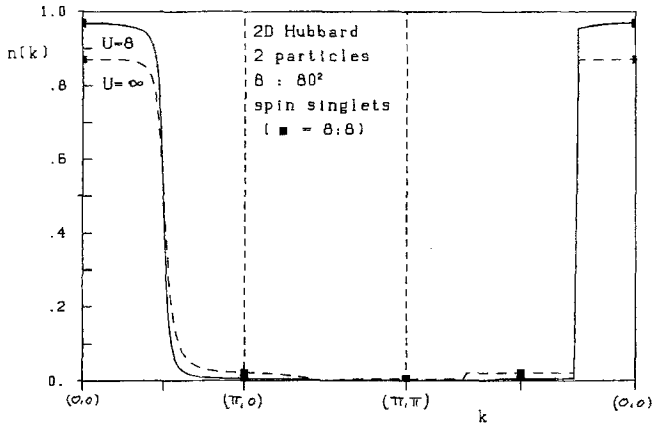

Fig. 9. The momentum distribution function, $n(\mathbf{k})$, for a 2D, Hubbard cluster, with 8 sites, $14400 = 120^2$ different boundary conditions and $N_e = 2$ particles. The smooth curves are the data for $n(\mathbf{k})$ along $(0,0) \rightarrow (\pi,0) \rightarrow (\pi,\pi) \rightarrow (0,0)$ in the Brillouin zone for $U = 8$ (continuous curve) and $U = \infty$ (long-dashed curve). Note the strong anisotropy of the (canonical) Fermi-edge. A sharp discontinuity along the (1, 1) direction ($\mathbf{k}_F \sim (\pi/4, \pi/4)$), and pseudo-insulating behaviour along the (1, 0) direction ($\mathbf{k}_F \sim (\pi/2, 0)$). Also shown (square symbols) are the data points for the corresponding 8:8 cluster (eight sites, periodic boundary conditions only)

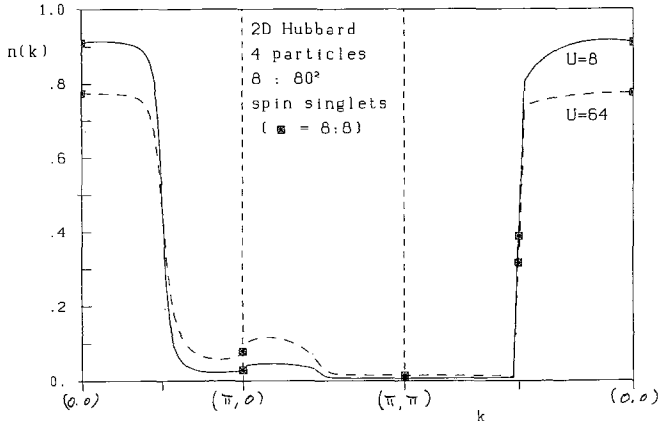

Fig. 10. The momentum distribution function, $n(\mathbf{k})$, for a 2D, Hubbard cluster, with 8 sites, $14400 = 120^2$ different boundary conditions and $N_e = 4$ particles. The smooth curves are the data for $n(\mathbf{k})$ along $(0,0) \rightarrow (\pi,0) \rightarrow (\pi,\pi) \rightarrow (0,0)$ in the Brillouin zone for $U = 8$ (continuous curve) and $U = 64$ (long-dashed curve). Note the strong anisotropy of the (canonical) Fermi-edge. A sharp discontinuity along the (1, 1) direction ($\mathbf{k}_F \sim (\pi/2, \pi/2)$), and pseudo-insulating behaviour along the (1, 0) direction ($\mathbf{k}_F \sim (\pi/2, 0)$). Also shown (square symbols) are the data points for the corresponding 8:8 cluster (eight sites, periodic boundary conditions only)

responds to a nominal density $n = 2/8 = 1/4$ and the (canonical) Fermi-surface includes therefore 1/8 of the Brillouin zone. We note a strong anisotropy in the behaviour of $n(k)$ near the *canonical* Fermi-edge. Along the (1, 1) direction, a discontinuity occurs at the Fermi-edge, here at $\sim(\pi/4, \pi/4)$. Along the (1, 0) direction $n(k)$ crosses *linearly* [17] the Fermi edge, here at $\sim(\pi/2, 0)$. An equivalent behaviour is also observed for the same eight-site cluster but with 4 particles, as shown in Fig. 10.

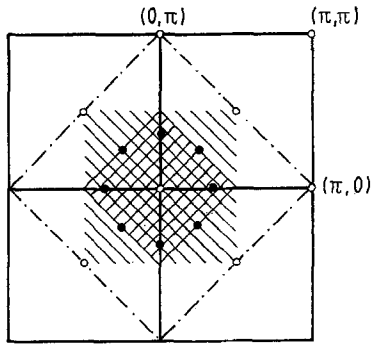

Fig. 11. An illustration of the eight-site system in momentum space. Shown are the positions (open circles) of the eight distinct momenta in the first Brillouin zone for the case of periodic boundary conditions. The volume inside the Fermi-surface for studies with fixed particle number (the *canonical* Fermi volume) is given by the square region cross-hatched (2 particles) and simply hatched (4 particles). For comparison we have included (full circles) the positions of the grand-canonical Fermi-edge along the (1, 1) and (1, 0) direction for $\mu = -2\sqrt{2}t$ in the $U = 0$ limit, which is retained in perturbation theory

In Fig. 11 we illustrate schematically the shape of the *canonical* Fermi-surfaces for the 8-site system with fixed number of particles $N_e = 2$ and $N_e = 4$ respectively. The open circles denote the position of the discrete momenta in the first Brillouin zone for the case of periodic boundary conditions. For the system with two interacting particles, the Fermi-surface is very close (though not identical) with the cross-hatched square region in Fig. 11. The simply hatched region (together with the cross-hatched region) in Fig. 11 is the approximate shape of the volume inside the Fermi-surface for the interacting 8-site system with fixed $N_e = 4$. Similarly, the Fermi surface is highly distorted with respect to its shape in noninteracting ($U = 0$) limit, as we will explain below.

The highly anisotropic Fermi-surfaces shown in Fig. 11 are due to the fact that the respective studies where done with fixed particle numbers. Such a study does *not* recover the non-interacting, $U = 0$, limit (of the extended lattice). In particular the exact shape of the Fermi-surface is not recovered for $U = 0$ (though the volume is correctly determined by the particle density). As an illustration of this phenomena we consider the example of 2 particles at $U = 0$ on the 8-site 2D cluster. We have confirmed numericaly that the Fermi-surface of the cluster with fixed $N_e = 2$ is given by the cross-hatched region in Fig. 11. Now we consider the *grand-canonical* formulation on the same 2D 8-site cluster. The particle number is now allowed to vary and the chemical potential, μ, is fixed. Clearly, for small $\mu \gtrsim -4t$ the particle numbers contributing to the grand-canonical average in (6) will be only $N_e = 0$ and $N_e = 2$. At a certain, critical μ_c fluctuations with $N_e = 4$ will start to contribute to (6). It is easy to show that $\mu_c = -2\sqrt{2}t$. Therefore $N_e = 0$ and $N_e = 2$ are sufficient to recover the non-interacting limit exactly for $\mu \in [-4t, -2\sqrt{2}t]$. In particular, also the shape of the Fermi-surface will be correctly described. For $\mu_c = -2\sqrt{2}t$ the Fermi edge lies at $\mathbf{k}_F = (\pi/4, \pi/4)$

along the (1, 1) direction. Along (1, 0) direction the Fermi edge has the form $\mathbf{k}_F=(k_x, 0)$, where k_x is the solution of

$$-2t(\cos k_x+1)=-2\sqrt{2}t, \tag{8}$$

or $k_x \sim 0.364\pi$. These values of k_F are denoted by the full circles in Fig. 11. Note that weak-coupling perturbation theory would not change these $\mathbf{k}_F$. Clearly, canonical and grand-canonical Fermi-surfaces differ dramatically and we conclude that a grand-canonical formulation is indispensable in a finite-size study of 2D Fermi-surface properties with the boundary-condition integration method at fillings $n<1$. Only at half-filling, $n=1$, do the canonical and grand-canonical Fermi-surfaces coincide.

Conclusions

We have presented fundamentals of the boundary condition integration technique [14] and applied it to the case of the Hubbard model in one- and two spatial dimensions [20]. In this model ferromagnetism occurs naturally at the Fermi surface which we suppressed by working in the subspace of spin-singlets. In 1D we find that for fillings smaller than one particle per site, this technique does not recover the Tomonaga-Luttinger liquid behaviour expected for the ground-state in the thermodynamic limit. Nevertheless, we gain substantially upon the estimate of the ground-state energy, when compared with the diagonalization of clusters with only periodic boundary conditions. In addition, a nearly continuous set of densities may be described with the boundary condition integration technique.

At half filling, details of the insulating behaviour for the ground-state are recovered both in 1D and 2D. The momentum distribution function, $n(k)$, shows no discontinuity at the Fermi-surface and passes linearly the Fermi surface. The finite size corrections to $n(k)$ are smaller than 5% even for small length chains in real space (eight sites). Off half filling we find in 2D, within the context of a canonical approach, large anisotropies and that the resulting *canonical* Fermi surface is strongly distorted with respect to the *grand-canonical* Fermi surface. We conclude that a grand-canonical formulation is important for finite-size studies of the 2D Hubbard and $t-J$ model.

In conclusion, we studied the boundary condition integration technique and showed that this technique extracts useful new information on Fermi-surface properties from exact diagonalization studies of finite clusters. It should be possible, in particular, to study the Mott-transition at half-filling and extract information on the shape of the Fermi-surface in 2D. Still, many open questions remain to be studied.

I would like to thank R. Valenti for carefully reading the manuscript, A.H. MacDonald for providing the basic frame of the program used for the diagonalization and S. Sorella for providing data on the 20-site chain. This work supported by the Minister für Wissenschaft und Forschung des Landes Nordrhein-Westfalen and by the European Community European Strategic Program for Research in Information Technology program, Project No. 3041-MESH. Part of the numerical calculations were done at the Hochleistungs-Rechenzentrum Jülich.

Appendix

Here we explain the simple projection technique used to enforce the constraint of a given total spin, usually the singlet contraint. Any wavefunction $|\psi\rangle$ for fermions with given spin on a finite lattice can be expanded in components of the total spin

$$|\psi\rangle=a_1|\psi_0\rangle+a_2|\psi_1\rangle+\ldots+a_{S_{\max}}|\psi_{S_{\max}}\rangle, \tag{9}$$

where the $|\psi_S\rangle$ are the components with fixed total spin, $\mathbf{S}^2_{\text{total}}|\psi_S\rangle=S(S+1)|\psi_S\rangle$ and $\mathbf{S}_{\text{total}}=\sum_i \mathbf{S}_i$. Clearly

$$|\psi'\rangle=(\mathbf{S}^2_{\text{total}}-S_{\max}(S_{\max}+1))|\psi\rangle \tag{10}$$

has no component of maximal spin $S_{\max}$. Iteration of Eq. (9) and Eq. (10) allows to project a given wavefunction on the subspace with a given total spin and perform the Lanzcos iterations within this subspace.

References

1. For a review see Solyom, J.: Adv. Phys. **28**, 201 (1979)
2. Haldane, F.D.M.: Phys. Rev. Lett. **45**, 1358 (1980); Haldane, F.D.M.: J. Phys. C**14**, 201 (1981)
3. Schulz, H.J.: Phys. Rev. Lett. **64**, 2831 (1990)
4. Kawakami, N., Yang, S.K.: Phys. Lett. A**148**, 359 (1990)
5. Frahm, H., Korepin, V.E.: Phys. Rev. B**42**, 10553 (1990)
6. Anderson, P.W.: Phys. Rev. Lett. **64**, 1839 (1990)
7. Engelbrecht, J.R., Randeira, M.: Phys. Rev. Lett. **65**, 1032 (1990)
8. Ogata, M., Shiba, H.: Phys. Rev. B**41**, 2326 (1990)
9. Sutherland, B.: Phys. Rev. B**12**, 3775 (1975); Schlottman, P.: Phys. Rev. B**36**, 5177 (1987); Bares, P.A., Blatter, G.: Phys. Rev. Lett. **64**, 2567 (1990)
10. Ogata, M., Luchini, M.U., Sorella, S., Assaad, F.F.: Phys. Rev. Lett. **66**, 2388 (1991)
11. Hellberg, C.S., Mele, E.J.: Phys. Rev. Lett. **67**, 2080 (1991)
12. Jullien, R., Martin, R.M.: Phys. Rev. B**26**, 6173 (1982)
13. Oles, A.M., Treglia, G., Spannjaard, D., Jullien, R.: Phys. Rev. B**32**, 2167 (1985)
14. Valenti, R., Gros, C., Hirschfeld, P.J., Stephan, W.: Phys. Rev. B**44** (1991)
15. Lin, H.Q., Campbell, D.K., Pan, C.Y.: Magnetic properties of the 2D Hubbard model at different band fillings (unpublished)
16. Horsch, P., Kaplan, T.A.: Bull. Am. Phys. Soc. **30**, 513 (1985); Yokoyama, H., Shiba, H.: J. Phys. Soc. Jpn. **56**, 1490 (1987)
17. We have confirmed this by diagonalizing clusters with boundary conditions which correspond to **k** values very near to the Fermi edge
18. Sorella, S.: Private communication
19. Imada, M., Hatsugai, Y.: J. Phys. Soc. Jpn. **58**, 3752 (1989)
20. In this study we considered only the one-band Hubbard model, since we wanted to connect to the $U=0$ limit, recovered exactly by the boundary condition technique. The generalization to the $t-J$ model is straightforward